Available online at www.sciencedirect.com
SciVerse ScienceDirect
Ceramics International 39 (2013) 13–20
CERAMICS INTERNATIONAL
www.elsevier.com/locate/ceramint

Review paper

Low-temperature synthesis of nanosized bismuth ferrite by the soft chemical method

E.C. Aguiar[a,1], M.A. Ramirez[b], F. Moura[c,2], J.A. Varela[a,1], E. Longo[a,1], A.Z. Simões[b,*]

[a] Universidade Estadual Paulista, UNESP, Instituto de Química,Rua Professor Francisco Degni s/n, CEP 14800-900, Araraquara, SP-Brazil
[b] Universidade Estadual Paulista, Unesp, Faculdade de Engenharia de Guaratinguetá, Av. Dr. Ariberto Pereira da Cunha, 333, Bairro Pedregulho, CEP 12516-410, Guaratinguetá-SP, Brazil
[c] Universidade Federal de Itajubá, Unifei, Campus Itabira, Rua São Paulo, 377, Bairro: Amazonas, CEP 35900-37, Itabira, MG, Brazil

Received 15 March 2012; received in revised form 25 May 2012; accepted 4 June 2012
Available online 12 June 2012

Abstract

This paper describes research on a simple low-temperature synthesis route to prepare bismuth ferrite nanopowders by the polymeric precursor method using bismuth and iron nitrates. $BiFeO_3$ (BFO) nanopowders were characterized by means of X-ray diffraction analyses, (XRD), Fourier transform infrared (FT-IR) spectroscopy, Raman spectroscopy (Raman), thermogravimnetric analyses (TG-DTA), ultra-violet/vis (UV/Vis) and field emission scanning electron microscopy (FE-SEM). XRD patterns confirmed that a pure perovskite $BiFeO_3$ structure with a rhombohedral distorted perovskite structure was obtained by heating at 850 °C for 4 hours. Typical FT-IR spectra for BFO powders revealed the formation of a perovskite structure at high temperatures due to a metal–oxygen bond while Raman modes indicated oxygen octahedral tilts induced by structural distortion. A homogeneous size distribution of BFO powders obtained at 850 °C for 4 hours was verified by FE-SEM analyses.

Keywords: A. Ceramics; B. Chemical syntheses; B. Powder metallurgy; C. X-Ray diffraction

Contents

1. Introduction

As a promising candidate for a high Curie temperature (T_C=850 °C) and high-ferroelectric performance. BFO nanopowder was the focus of attention in the 1960s–1970s [1–6].

*Corresponding author. Tel.: 55 12 3123 2765.
E-mail address: alezipo@yahoo.com (A.Z. Simões).
[1] Tel.: +55 16 33019828.
[2] Tel.: +55 31 3834 6472/6136; fax: +55 31 3834 6472/6136.

0272-8842/$36.00
http://dx.doi.org/10.1016/j.ceramint.2012.06.014

Its ferroelectric phase structure [7] shows huge shifts of Bi^{3+} and Fe^{3+} ions, as well as counter rotations of oxygen octahedrons along the (111) direction from the non-ferroelectric centro-symmetric cubic structure which produces the R3c space group and a very high spontaneous electric polarization (*Ps*) as calculated from the structural data. BFO is also a multiferroic material with an antiferromagnetic ordering which occurs below the Néel temperature (T_N 310–370 °C) (there are discrepancies regarding T_N, measured by different authors with different methods) [8,9]. The magnetic structure of BFO is a *G*-type [10] with a cycloidal spiral arrangement of the magnetic moments of Fe^{3+} ions [11], and the canted spins arising from the Dzyaloshinskii–Moriya (D–M) interaction [12] result in weak ferromagnetism in BFO. Although great achievements have been made in the preparation of BFO thin films by the pulsed-laser deposition (PLD) method [13], it is difficult to avoid the formation of impurity phases by the conventional solid-state reaction in bulk materials. BFO perovskites can stabilize only within a narrow temperature range. To date, the synthesis of single-phase BFO crystallites or ceramics is still a challenging issue. In the solid-state route, nitric acid leaching was required to eliminate impurity phases such as $Bi_2Fe_4O_9$ and $Bi_{25}FeO_{40}$, after the calcination of mixed bismuth and iron oxides [14], which resulted in coarser powders and the poor reproducibility. Most recently, Wang [15] and Pradhan et al. [16] prepared the pure phase of BFO ceramics by a rapid liquid-phase sintering technique. The required BFO crystallization temperature was above the ferroelectric Curie temperature T_c, which implies that the volatilization of bismuth was hard to avoid. Moreover, Ghosh et al. [17] produced phase pure BFO nanopowders by the tartaric acid based sol–gel method coupled with an additional calcination process. The preparation of a polycrystalline pure phase BFO is reported to be difficult because of its narrow temperature range of phase stabilization. Various impurity phases have been reported to occur which are mainly comprised of $Bi_2Fe_4O_9$, $Bi_{12}(Bi_{0.5}\ Fe_{0.5})O_{19.5}$ and $Bi_{25}FeO_{40}$ [18]. These impurities cause a high leakage current which leads to poor ferroelectric behavior. The most common techniques developed for the formation of pure phase polycrystalline BFO powders are (a) formation of a BFO solid solution with other ABO_3 perovskites types such as $BaTiO_3$ [19]; (b) calcination followed by leaching with nitric acid [20], (c) microwave assisted hydrothermal [21]; (d) rapid liquid phase sintering of BFO [22]; and (e) use of rather expensive but ultrapure starting powders of Bi_2O_3 and Fe_2O_3 or with a slight deficiency of Bi_2O_3 [23].

Although several attempts have been made to prepare BFO crystallites, few researchers have studied the formation of perovskite BFO by the polymeric precursor method at several annealing temperatures. Our group has expended significant effort to develop synthetic routes to fabricate single-phase lanthanum modified $BiFeO_3$ (BFO) powders by the polymeric precursor method [24,25]. Our data confirmed that a perovskite phase was synthesized at a temperature of 850 °C for 2 h while infrared data indicates no trace of carbonate. A structural phase transition from rhombohedral to orthorhombic is observed near x=0.30. X-ray absorption near-edge structure (XANES) spectra revealed iron atoms in a 3+ valence state while SEM analysis confirmed structural distortion leading to a different grain shape after the lanthanum addition. Lower leakage current density and superior ferroelectric hysteresis loops at room temperature were noted with an increase in the lanthanum content. The advantage of the soft chemical route is that nanocrystallites can be synthesized at a much lower temperature with energy saving and cost effectiveness. The overall process consists of preparing a solution based on metallic citrate polymerization and eliminating the organic material to synthesize the desired phase. In this study, the effect of the annealing temperature on the phase formation, crystal structure and the morphology of BFO ceramics prepared by polymeric precursor method was investigated.

2. Experimental details

Based on the polymeric precursor method (the Pechini method) [26], the BFO synthesis procedure is associated with the fact that certain α-hydroxycarboxylic organic acids can form polybasic acid chelates with a wide range of cations. After the addition of a polyethylene glycol and heating, the chelate transforms into a polymer with a homogeneous cation distribution. Iron (III) nitrate nonahydrate (Merck) and bismuth nitrate (Aldrich) were used as raw materials. Precursor solutions of bismuth and iron were prepared by adding the raw materials to ethylene glycol and an aqueous citric acid concentrate under heating and stirring. Appropriate quantities of Fe and Bi solutions were mixed and homogenized by stirring at 90 °C. The molar ratio of metal:citric acid:ethylene glycol was 1:4:16. In this study, an excess of 5 wt% Bi_2O_3 was added to the solution to compensate for unavoidable bismuth oxide loss during thermal treatment. Without the addition of excess bismuth oxide, a pure phase could not be obtained [27]. Pure BFO was prepared from the metal citrate complex which was polyesterified in ethylene glycol. Most of the organic matter was subsequently eliminated at temperatures as low as 300 °C, and a dark residue containing reactive oxides with well-controlled stoichiometry was formed. The formed porous product was crushed and heated in an alumina crucible from 600 to 850 °C for 4 hours (BFO600, BFO700, BFO800, BFO850) to eliminate organic material residues.

Powders were analyzed by XRD for phase determination. For Rietveld analyses, XRD data were collected with a Rigaku 20-2000 diffractometer under the following experimental conditions: 40 kV, 30 mA, $20^\circ \leq 2\theta \leq 100$, $\Delta 2\theta = 0.02^\circ$, λCu k_α monochromatized by a graphite crystal with a divergence slit of 2 mm, a reception slit of 0.6 mm and a step time of 10 s. The Rietveld analysis was performed with the Rietveld refinement program DBWS-941 1 [28]. A modified Thompson–Cox–Hasting pseudo-Voigt profile function was used where η (the lorentzian fraction of the function) varies with the Gauss and Lorentz components of the full width at half maximum. TG-DTA analyses were carried out using a Netzsch-409 STA apparatus with a heating rate of 20 °C min^{-1} under flowing air from room temperature to 1000 °C. FT-IR spectra were recorded with a Bruker Equinox-55 instrument. Raman spectra were collected using a Bruker RFS-100/S Raman spectrometer with Fourier transform. A 1064 nm YAG laser was used as the excitation source, and its power was maintained at 150 mW. Band gap values were obtained using ultraviolet spectrosocopy in the visible region curve (UV–vis–NIR Spectrophotometer-VARIAN Cary 500 X). Microstructural characterization was performed by FE-SEM (Supra 35-VP, Carl Zeiss, Germany).

3. Results and discussion

3.1. X-ray diffraction analyses

Fig. 1 shows the diffraction patterns of thermally treated powders at temperatures between 600 and 850 °C. The formed perovskite must have a composition close to $BiFeO_3$. At the lowest tested temperature (600 °C), a mixture of initial precursors and a perovskite-structured material was obtained. At 800 °C, the material is practically formed by the perovskite phase without any traces of a secondary phase identified as $Bi_2Fe_4O_9$ (JCPDS 20-0836-marked with ∗ in Fig. 1a), which is commonly observed in this system [29]. The formation of $Bi_2Fe_4O_9$ by Bi evaporation can be ruled out. Chen et al. [30] detected this phase after heating at 160–180 °C where Bi evaporation is not possible. Other authors state that this phase is a consequence of the decomposition of $BiFeO_3$. Recently, Selbach et al. [31] described how this secondary phase is formed at 600–800 °C by the decomposition of BFO and disappears at higher temperatures because Bi and Fe are incorporated into the structure. They rule out any effect of Bi evaporation as traces would exist at increased temperatures or even in higher amounts which was not the case. Thus, a decrease in the synthesis temperature with respect to the temperature required by the classical solid state reaction method (850–900 °C) [32] is obtained. The lowering of the synthesis temperature is equivalent to sol–gel method values [33]. Patterns show that initially a bismuth rich phase of $Bi_xFe_yO_{1.5x+1.5y}$ ($x > y$) composition forms at a temperature of 600 °C followed by the evolution of a $BiFeO_3$ phase at 700 °C. Calcination between temperatures of 700–850 °C suggest that the impurity phase is completely eliminated at any of these temperatures. What is more remarkable is that the amount of the secondary phase is considerably reduced in samples synthesized by the polymeric precursor method (even at low temperatures) which appears to stem from the complexation process which induced effects in the samples and enhanced the perovskite-structured $BiFeO_3$ formation. Fig. 1(d) shows that BFO thermally treated at 850 °C for 4 hours exhibits a pure R3c structure without any impurity. The lattice parameters calculated from XRD patterns are $a = 5.6206$ Å and $c = 13.6924$ Å.

XRD data reveal that $BiFeO_3$ was obtained with a rhombohedral distorted perovskite structure by the polymeric precursor method (see Fig. 2). In this study, we have adopted the Rietveld refinement technique to investigate the crystal structure of BFO nanopowders. Data were collected from powders calcinated at 850 ºC for 4 hours. Table 1 illustrates the R_{wp}, R_{exp} and S indices as well as lattice parameters (a and c) and the unit cell volume (V). Atomic positions obtained by Rietveld analyses belong to the ICSD card (86-1518). Quantitative phase analyses of powders for the rhombohedral distorted phase were calculated according to Young [28]. Obtained results confirm that the covalent interaction which originates from the strong hybridization between Fe 3d and O 2p orbitals plays an important role in the structural distortion of the BFO lattice at high temperatures. From the low S values ($S = R_{wp}/R_{exp}$), it can be assumed that the refinement

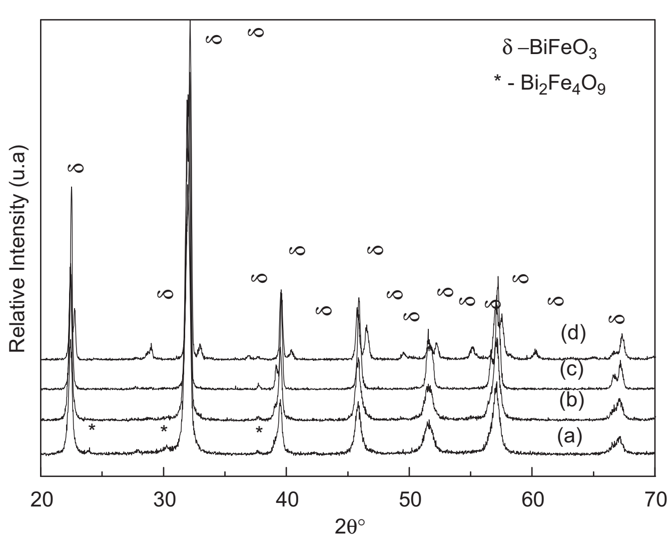

Fig. 1. XRD pattern of a BFO nanopowders thermally treated at (a) 600 °C (b) 700 °C (c) 800 °C and (d) 850 °C for 4 hours by the polymeric precursor method.

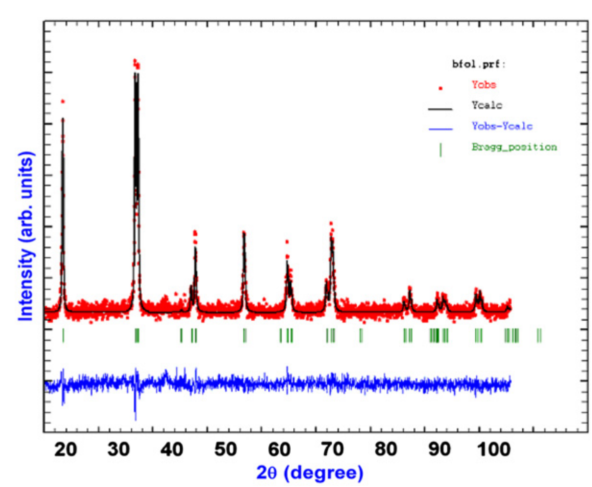

Fig. 2. Rietveld refinement of a BFO nanopowders thermally treated at 850 °C for 4 hours.

Table 1
E.C. Aguiar, M.A. Ramirez, F. Moura, J.A. Varela, E. Longo, A.Z. Simões.

	Parameter	BFO
Refinement index	R_{wp} (%)	11.12
	R_{exp}	7.06
	S	1.57
Atomic positions	A1	0; 0; 0.06722
	A2	0; 0; 0.21091
	B1	0; 0; ½
	B2	0; 0; 0.37099
	O1	¼; ¼; 0
	O2	¼; ¼; ¼
	O3	0; 0; 0.43786
	O4	0; 0; 0.32536
	O5	¼; ¼; 0.11165
S_{Occ}	Bi (A1)	1.00000
	La (A1)	0.00000
	O	0.91700
Lattice parameter	a (Å)	5.6206
	c (Å)	13.6924
	V (Å^3)	374.57
	t	0.915
Perovskite (mol%)	97.5 ± 0.5	
Stoichiometry	$BiFeO_3$	
Refinement	$BiFeO_{2.6}$	

was successfully performed with all the investigated parameters close to literature data [34].

3.2. Thermal analyses

To determine the best annealing conditions and to evaluate the crystallization temperature necessary to obtain a single BFO phase, thermal analyses were performed. Two stages corresponding to the weight and energy change are visible (see Fig. 3). The first characterized stage (25–200 °C) with a small weight loss is related to the elimination of excess ethylene glycol and water formed during the esterification process. The second stage (380–650 °C) corresponds to the decomposition of polymeric metal–carboxylate complexes and to the formation of a metal oxide phase. The DTA curve shows two strong exothermic peaks at around 400–420 °C and 600–650 °C which corresponds to a weight loss that must be considered as the crystallization of the residual amorphous phase and the decomposition of the polymeric metal–carboxylate complexes. Preceded by the impurity phase, the formation of BFO occurs at 580–600 °C as suggested by weight loss as well as a weak endothermic peak in the DTA curve which is also confirmed by XRD patterns (see Fig. 1(a)).

3.3. FT-IR, Raman and UV–vis analyses

FT-IR spectra of crystalline BFO nanopowders derived from the polymeric precursor method are shown in Fig. 4. The broad band at 3000–3600 cm^{-1} is due to the

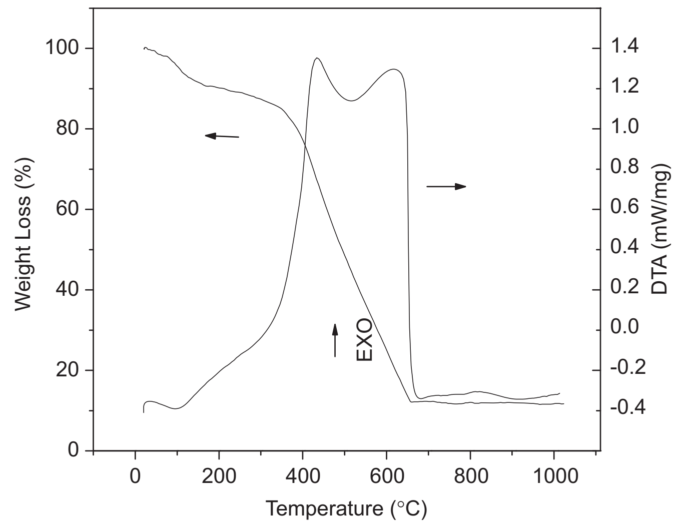

Fig. 3. TG/DTA curves of a BFO resin thermally treated at 300 °C for 4 hours by the polymeric precursor method.

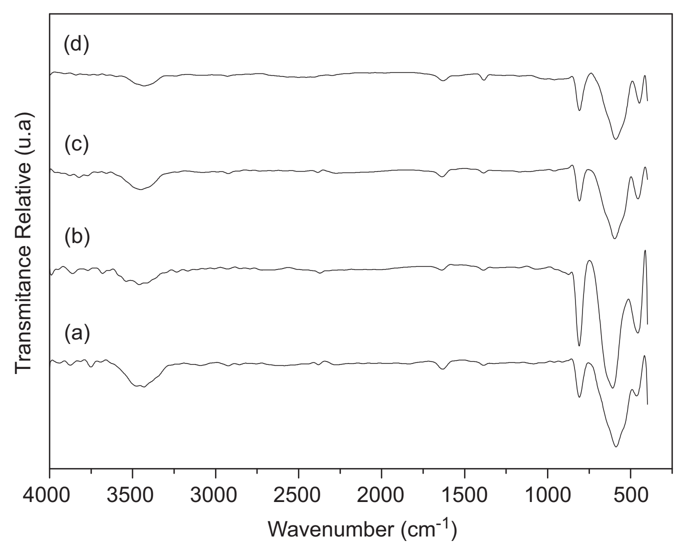

Fig. 4. (a) FT-IR spectra of a BFO nanopowders thermally treated at (a) 600 °C (b) 700 °C (c) 800 °C and (d) 850 °C for 4 hours by the polymeric precursor method.

antisymmetric and symmetric bond stretching of H_2O and OH^- groups while a band at 1630 cm^{-1} corresponds to bending vibrations of H_2O [35]. Specifically, strong absorptive peaks at 400–600 cm^{-1} are attributed to the Fe–O stretching and bending vibration which are characteristics of octahedral FeO_6 groups in perovskite compounds. The formation of a perovskite structure can be confirmed by the presence of a metal–oxygen bond [36]. Residual water and a hydroxy group are usually detected in the as-grown samples; further heat treatment is required for their elimination. The hydroxylation of metal ions and deprotonation can be accelerated by raising the solution temperature or pressure [37]. However, there was a vibration band associated with the deformation of O–H bonds near 1680 cm^{-1} which is attributed to water adsorbed at the powder surface when the sample was in contact with the environment. Crystallized powders were found to have OH^- ions under the present sample preparation conditions. Furthermore, the hydroxyl content was found to decrease with increased annealing temperatures which could be due to the vigorous action of annealing conditions to remove these groups at elevated temperatures. The band at around 830 cm^{-1} was due to traces of trapped NO_3^- ions in BFO nanopowders [38]. BFO nanopowders contain a few traces of carbonates (C=O vibration around 1450 cm^{-1}) independent of the annealing temperature which suggests that the nanopowder surface was in contact with the CO_2 environment. This problem should be minimized during the sample preparation since many properties are dependent on the purity of the raw powders (especially carbonate traces) which can result in porous ceramics due to CO_2 elimination.

Raman scattering has proven to be a valuable technique to obtain information about local structures within materials. Fig. 5a–d shows Raman spectra for BFO nanopowders derived at different annealing temperatures. The degree of order–disorder in the crystal lattice of BFO nanopowders at short and medium distances was investigated. Modes located at 212, 316, 377, 445, 537 and 635 cm^{-1} are caused by the internal vibration of FeO_6 octahedra whereas modes below 200 cm^{-1} must be attributed to different sites occupied by bismuth within perovskite units. Bands located at 97, 120 and 145 cm^{-1} are related to Bi atoms of the perovskite layer which corresponds to a rigid layer. These modes are probably due to a distortion in the A site caused by the bismuth ion. This distortion into the A site of perovskite enhances the Jahn–Teller distortion of FeO_6 octahedra. On the other hand, Raman modes located above 200 cm^{-1} are responsible for distortions and vibrations of FeO_6 octahedra. As the temperature decreases, there is a reduction in the Raman band intensities (mainly the mode located at 209 cm^{-1}) which is due to Fe–O atom vibrations inside the perovskite layer and to vibrations of Bi–O atoms within the Bi_2O_2 layer. The appearance of a Raman mode at low frequency (97 cm^{-1}) is due to the Bi ion atomic mass which causes Bi displacements in the Bi_2O_2 layer. All Raman modes can be indexed to the modes of a BFO molecule with a R3c structure [39]. BFO850 and BFO800 show almost identical curves except that the intensity of A_1 and E_3 modes for BFO850 is significantly stronger than the intensity of BFO-800. As indicated by Simões et al. [40], the shift of Raman peaks higher than 200 cm^{-1} results from the FeO_6 octahedron. The stronger intensity of A_1 and E_3 modes for BFO850 can be attributed to the oxygen octahedral tilt-induced structural distortion. Raman results are in agreement with XRD data which indicates an ordered structure at short and long distances.

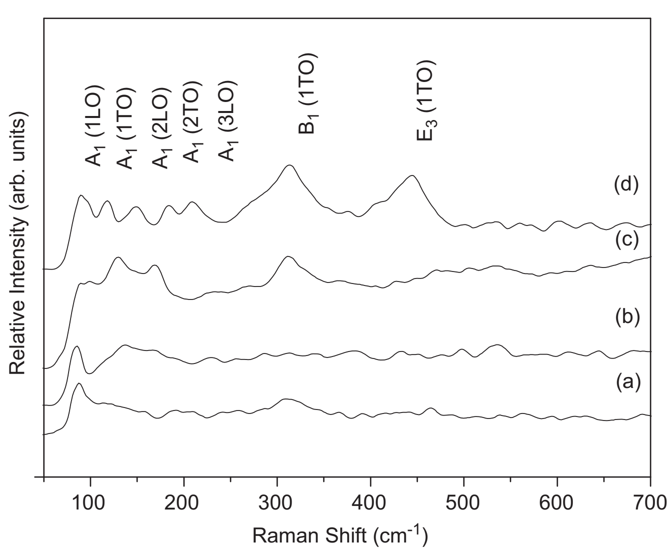

Fig. 5. (a) Raman spectra of a BFO nanopowders thermally treated at (a) 600 °C (b) 700 °C (c) 800 °C and (d) 850 °C for 4 hours by the polymeric precursor method.

Fig. 6 shows the UV–vis optical diffuse absorbance spectra of BFO nanopowders thermally treated at different temperatures. The respective band gap values determined from the Kubelka model [41]. The optical energy band gap is related to the absorbance and to the photon energy by the following Eq. (1):

$$h\nu\alpha\mu(h\varrho - E_g{}^{opt})^2 \quad (1)$$

where α is the absorbance, h is the Planck constant, v is the frequency and E_g^{opt} is the optical band gap [42]. Values obtained are 3.04, 2.97, 2.95, 2.89, respectively. Our BFO nanopowders exhibited characteristic absorption spectra of ordered or crystalline materials. These results indicate that the exponential optical absorption edge and the optical band gap are controlled by the degree of structural disorder in the BFO lattice. This decrease in the band gap value as the temperature increases can be ascribed to a reduction of defects in the lattice which decreases intermediary energy levels due to the reduction of oxygen vacancies located at BO_6^- octahedra. The main differences in optical band gaps can be related to different factors which mainly include: the synthesis method, shape (powder, crystal or thin film) and synthesis conditions. The reflectance significantly decreases near the excitonic absorption edge as the temperature changes which is related to the optical band gap. The decrease in the band gap with increased temperature might be explained by the suppressed tilt angle of the oxygen octahedra which increases the Fe^{2+}–O–Fe^{3+} angle. Forced higher symmetry is expected to increase the band width of occupied and unoccupied bands which reduces the band gap [43]. The band gap obtained in our study is higher than the reported value of about 2.67 eV for bulk $BiFeO_3$ [44] which might be due to the size effect [45].

3.4. FE-SEM analyses

The effect caused by the annealing temperature on the morphology and shape of nanopowders was evaluated by

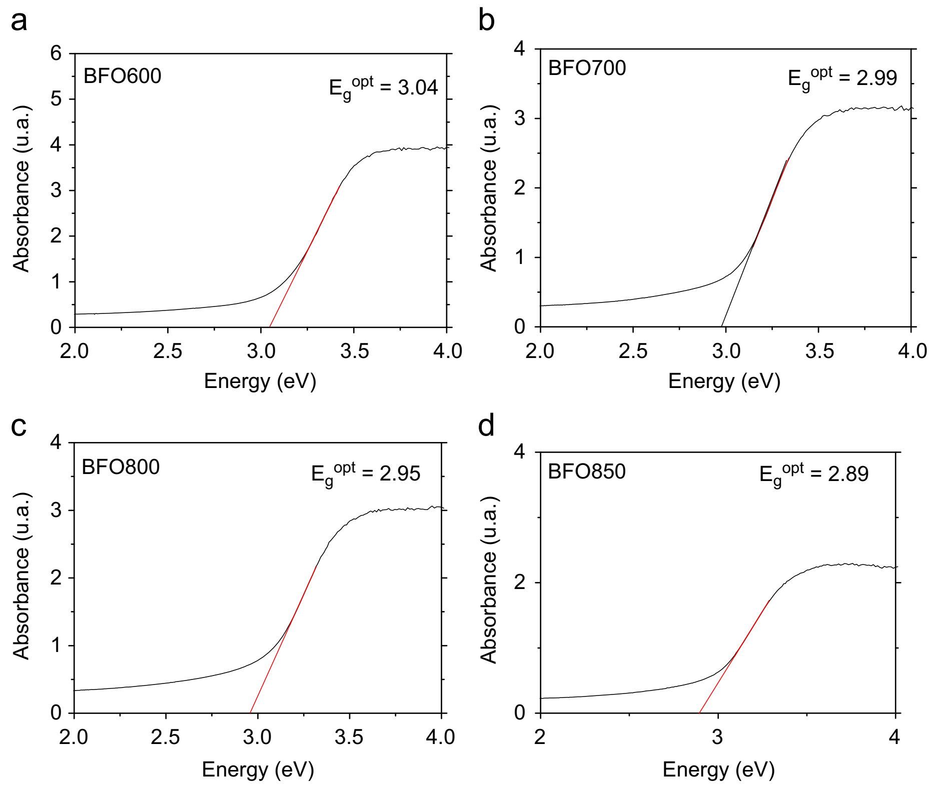

Fig. 6. UV–vis of a BFO nanopowders thermally treated at (a) 600 °C (b) 700 °C (c) 800 °C and (d) 850 °C for 4 hours by the polymeric precursor method.

FE-SEM analyses (see Fig. 6). Fig. 7 Increasing the temperature had a pronounced effect on the nanopowder shape which leads to a plate-like morphology and a structural distortion (see inset of Fig. 6d). The change in the particle size varies from 35 to 60 nm as the temperature increases. BFO nanopowders thermally treated at 600 °C present a rod-like morphology with particles of around 35 nm. Rod-like grains might originate from the anisotropic behavior of bismuth ferrite. The nanopowder size is heterogeneously distributed with a rod-like morphology form which is different from literature data [46]. According to the image, most BFO nanopowders thermally treated at low temperatures reveal a few large particles with an irregular shape. The nanopowder morphology variation may indicate the formation of impurity phases. Submicron and isotropy BFO crystallites obtained in our study are quite different from the previous research where BFO nanopowders agglomerated into a cube with a side size of 45 using the microwave assisted hydrothermal (MAH) method [47]. In our case, a critical annealing temperature existed where the formation of impurity phases was favored, and the formation of pure BFO was highly dependent upon it. Increasing the annealing temperature, causes Bi^{3+} and Fe^{3+} to react at high temperatures. If temperature conditions are carefully maintained during the experiment, neither etching of BFO crystals nor the formation of a second phase will occur. Therefore, the crystallization process continued in such a way that the system was self-stabilizing. We conjecture that the dissociation of bismuth and iron during annealing and the formation of ionic complexes might prevent the growth of BFO crystallites and limit the size of BFO particles to the nanometric range. The agglomeration process was attributed to van der Waals forces. To reduce the surface energy, primary particles have a tendency to form nearly spherical agglomerates in a minimum surface-to-volume ratio and hence reduce surface free energy. This type of grain structure is common in oxide, ferrite and titanate ceramics [48].

4. Conclusions

A simple method was used to prepare pure BFO nanopowders which are free of impurities at a temperature of 850 °C for 4 hours. A better homogeneity of nanopowders is obtained at this temperature. The stability of the perovskite phase increases at high temperatures. A longer annealing temperature was beneficial to inhibit the formation of any impurity phases and promote the growth of BFO crystallites into single-phase perovskites. Rietveld refinement reveals a rhombohedral distorted structure with a space group of R3c. The polymeric precursor method is important not only for the low temperature crystallization of BFO nanopowders, but also for controlling morphological and structural properties. Therefore, this method is undeniably a genuine technique for low temperatures in comparison with solid state reactions.

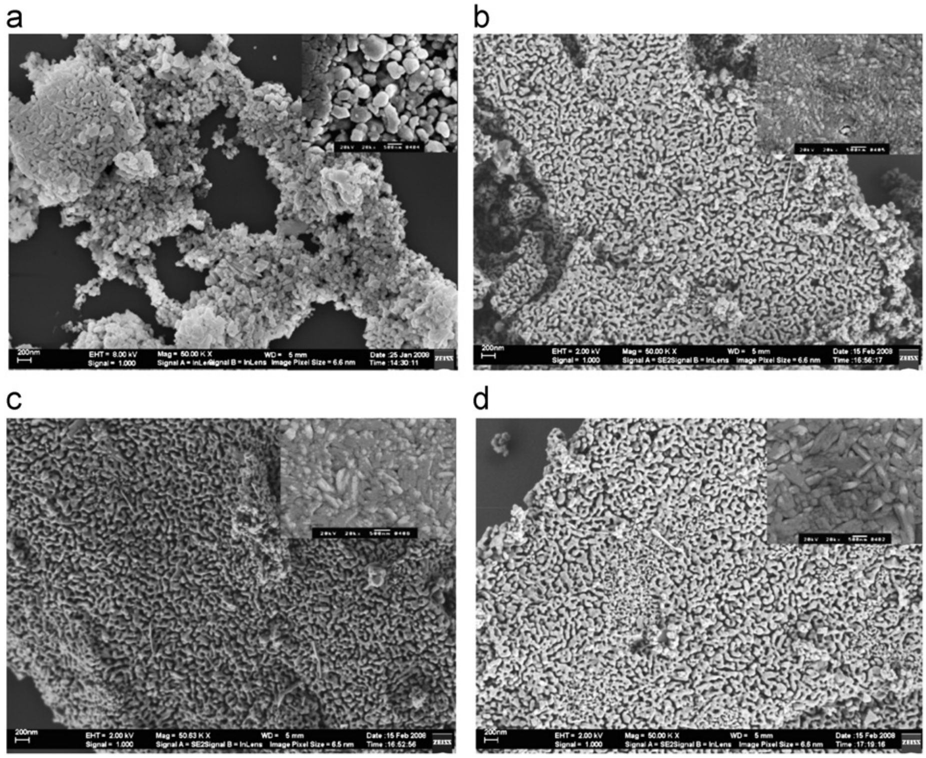

Fig. 7. FE-SEM images and inset of a BFO nanopowders thermally treated at (a) 600 °C (b) 700 °C (c) 800 °C and (d) 850 °C for 4 hours by the polymeric precursor method.

Acknowledgments

The authors gratefully acknowledge the financial support of the Brazilian agencies FAPESP, CNPq and CAPES.

References

[1] E.K.H. Salje, Phase Transitions in Ferroelectrics Ferroelastic and Coelastic Crystals, Cambridge University Press, Cambridge. http://dx.doi.org/10.1063/1.2168038.

[2] V.E. Wood, A.E. Austin, Possible applications for magnetoelectric materials, International Journal of Magnetism 5 (1974) 303–315.

[3] N.A. Hill, Why are there so few magnetic ferroelectrics? The Journal of Physical Chemistry B 104 (2000) 6694–6697.

[4] G.A. Smolenskii, V.M. Yudin, Antiferromagnetic properties of some perovskite, Soviet Physics—JETP 16 (1963) 622–624.

[5] C. Michel, J.M. Moreau, G.D. Achenbach, R. Gerson, W.J. James, The atomic structure of $BiFeO_3$, Solid State Communications 7 (1969) 701–704.

[6] J.R. Teague, R. Gerson, W.J. James, Dielectric hysteresis in single crystal $BiFeO_3$, Solid State Communications 8 (1970) 1073–1074.

[7] F. Kubel, H. Schmid, Structure of a ferroelectric and ferroelastic monodomain crystal of the perovskite $BiFeO_3$, Acta Crystallographica, Section B: Structural Crystallography and Crystal Chemistry 46 (1963) 610–616.

[8] G. Smolenskii, New ferroelectrics of complex composition, Soviet Physics—Solid State 2 (1961) 2651–2654.

[9] S.V. Kiselev, R.P. Ozerov, G.S. Zhdanov, Detection of magnetic order in ferroelectric $BiFeO_3$ by neutron diffraction, Soviet Physics—Doklady 7 (1963) 742–744.

[10] I. Sosnowska, T. Peterlin-Neumaier, E. Steichele, Spiral magnetic ordering in bismuth ferrite, Journal of Physics C: Solid State Physics 15 (1982) 4835–4846.

[11] I.E. Dzialoshinskii, Thermodynamic theory of Weak" ferromagnetism in antiferromagnetic substances, Soviet Physics—JETP 5 (1957) 1259–1262.

[12] J. Wang, J.B. Neaton, H. Zheng, V. Nagarajan, S.B. Ogale, B. Liu, D. Viehland, V. Vaithyanathan, D.G. Schlom, U.V. Waghmare, N.A. Spaldin, K.M. Rabe, M. Wuttig, R. Ramesh, Epitaxial $BiFeO_3$ multiferroic thin film heterostructures, Science (New York, NY) 299 (2003) 1719–1722.

[13] K.Y. Yun, M. Noda, M. Okuyama, H. Saeki, H. Tabata, K. Saito, Structural and multiferroic properties of $BiFeO_3$ thin films at room temperature, Journal of Applied Physics 96 (2004) 3399–3404.

[14] M. Mahesh Kumar, V.R. Palkar, K. Srinivas, S.V. Suryanarayana, Ferroelectricity in a pure $BiFeO_3$ ceramic, Applied Physics Letters 76 (2000) 2764–2766.

[15] Y.P. Wang, L. Zhou, M.F. Zhang, X.Y. Chen, J.M. Liu, Z.G. Liu, Synthesis of bismuth ferrite nanoparticles via a wet chemical route at low temperature, Applied Physics Letters 84 (2004) 1731–1733.

[16] A.K. Pradhan, K. Zhang, D. Hunter, J.B. Dadson, G.B. Loutts, Magnetic and electrical properties of single-phase multiferroic $BiFeO_3$, Journal of Applied Physics 97 (2005) 093903–093908.

[17] S. Ghosh, S. Dasgupta, A. Sen, H. Sekhar, Low-temperature synthesis of nanosized bismuth ferrite by soft chemical route, Journal of the American Ceramic Society 88 (2005) 1349–1352.

[18] V.R. Palkar, R. Pinto, Colossal magnetoresistance and other materials, Pramana Journal of Physics 58 (2002) 1003–1008.

[19] R.T. Smith, G.D. Achenbach, R. Gerson, W.J. James, Dielectric properties of solid solutions of $BiFeO_3$ with $Pb(Ti,Zr)O_3$ at high temperature and high frequency, Journal of Applied Physics 39 (1968) 70–74.

[20] V.V. Shvartsman, W. Kleemann, R. Haumont, J. Kreisel, Large bulk polarization and regular domain structure in ceramic $BiFeO_3$, Applied Physics Letters 90 (2007) 172115–172123.

[21] Y.P. Wang, L. Zhou, M.F. Zhang, X.Y. Chen, J.M. Liu, Z.G. Liu, Room-temperature saturated ferroelectric polarization in $BiFeO_3$ ceramics synthesized by rapid liquid phase sintering, Applied Physics Letters 84 (2004) 1731–1733.

[22] M. Kumar, K.L. Yadav, Large magnetization in Mn doped $BiFeO_3$ ceramics with enhanced polarization and weak magnetization, Applied Physics Letters 91 (2007) 112911–112913.

[23] M. Valant, A.-K. Axelsson, N. Alford, Peculiarities of a solid-state synthesis of multiferroic polycrystalline $BiFeO_3$, Chemistry of Materials : A Publication of the American Chemical Society 19 (2007) 5431–5436.

[24] F. Gonzalez Garcia, C.S. Riccardi, A.Z. Simões, Lanthanum doped $BiFeO_3$ powders: syntheses and characterization, Journal of Alloys and Compounds 501 (2010) 25–29.

[25] A.Z. Simões, F. Gonzalez Garcia, C.S. Riccardi, Rietveld analysys and electrical properties of lanthanum doped $BiFeO_3$ ceramics, Materials Chemistry and Physics 116 (2009) 305–309.

[26] M. Pechini**,** Method of Preparing Lead and Alkaline Earth Titanates and Niobates and Coating Method Using the Same to Form a Capacitor, U.S. Patent no. Mat3.330.697, 1967.

[27] M.A. Zaghete, C.O. Paiva-Santos, J.A. Varela, E. Longo, Y.P. Mascarenhas, Chemical synthesis of PZT powder by autocombustion of citrate-nitrate gel, Journal of the American Ceramic Society 75 (1992) 2089–2093.

[28] R.A. Young, A. Sakthivel, T.S. Moss, C.O. Paiva-Santos, An upgrade of the DBWS*.* Programms for Rietveld refinement with PC and mainframe computers, Journal of Applied Crystallography 28 (1995) 366–367.

[29] L.Y. Wang, D.H. Wang, H.B. Huang, Z.D. Han, Q.Q. Cao, B.X. Gu, Y.W. Du, The magnetic properties of polycrystalline $Bi_{1-x}Sr_xFeO_3$ ceramics, Journal of Alloys and Compounds 469 (2009) 1–3.

[30] C. Chen, J. Cheng, S. Yu, L. Che, Z. Meng, Development of new NLO Crystals for UV and IR applications, Journal of Crystal Growth 291 (2006) 135–139.

[31] S.M. Selbach, M.A. Einarsrud, T. Grande, On the thermodynamic stability of $BiFeO_3$, Chemistry of Materials : A Publication of the American Chemical Society 21 (2009) 169–173.

[32] V.A. Khomchenko, V.V. Shvartsman, P. Borisov, W. Kleemann, D.A. Kiselev, I.K. Bdikin, J.M. Vieira, A.L. Kholkin, Effect of Gd-substitution on the crystal structure and multiferroic properties of $BiFeO_3$, Acta Materialia 57 (2009) 5137–5145.

[33] J. Wei, D. Xue, Enhanced ferromagnetic properties of multiferroic $Bi_{1-x}Sr_x$Mn0.2$Fe_{0.8}O_3$ synthesized by sol–gel process, Electrochemical and Solid State Letters 10 (2007) G85–G88.

[34] S. Luo, Y. Noguchia, M. Miyayamab, T. Kudo, Rietveld analysis and dielectric properties of Bi_2WO_6-$Bi_4Ti_3O_{12}$ ferroelectric system, Materials Research Bulletin 36 (2001) 531–540.

[35] A.Z. Simões, B.D. Stojanovic, M.A. Ramirez, A.A. Cavalheiro, E. Longo, J.A. Varela, Lanthanum-doped $Bi_4Ti_3O_{12}$ prepared by the soft chemical method: Rietveld analysis and piezoelectric properties, Ceramics International 34 (2008) 257–261.

[36] D. Lee, M.G. Kim, S. Ryu, H.M. Jang, S.G. Lee, Epitaxially grown La modified $BiFeO_3$ magnetoferroelectric thin films, Applied Physics Letters 86 (2005) 222903–229905.

[37] H. Wang, J.J. Zhu, J.M. Zhu, X.H. Liao, S. Xu, T. Ding, Preparation of nanocrystalline ceria particles by sonochemical and microwave assisted heating methods, Physical Chemistry 4 (2002) 3794–3799.

[38] H. Zhang, X. Fu, S. Niu, Q. Xin, Synthesis and luminescent properties of nanosized YVO_4:Ln (Ln = Sm, Dy), Journal of Alloys and Compounds 457 (2008) 61–65.

[39] Y. Yang, J.Y. Sun, K. Zhu, Y.L. Liu, L. Wan, Increased efficiency of low band gap polymer solar cells at elevated temperature and its origins, Journal of Applied Physics 103 (2008) 093532–093537.

[40] A.Z. Simões, E.C. Aguiar, A.H.M. Gonzalez, J. Andrés, E. Longo, J.A. Varela, Strain behavior of lanthanum modified $BiFeO_3$ thin films prepared via soft chemical method, Journal of Applied Physics 104 (2008) 104115–104120.

[41] P. Kubelka, F. Munk, Ein Beitrag Zur Optik der Farbanstriche, Zeitschrift für Technische Physik 12 (1931) 593–601.

[42] D.L. Wood, J. Tauc, Week absorption tails in amorphous semiconductors, Physical Review B 5 (1972) 3144–3151.

[43] A.Y. Borisevich, H.J. Chang, M. Huijben, M.P. Oxley, S. Okamoto, M.K. Niranjan, J.D. Burton, E.Y. Tsymbal, Y.H. Chu, P. Yu, R. Ramesh, S.V. Kalinin, S.J. Pennycook, Suppression of cctahedral tilts and associated changes in electronic properties at epitaxial oxide heterostructure interfaces, Physical Review Letters 105 (2010) 087204–087207.

[44] P. Chen, N.J. Podraza, X.S. Xu, A. Melville, E. Vlahos, V. Gopalan, R. Ramesh, D.G. Schlom, J.L. Musfeldt, Optical properties of quasi-tetragonal $BiFeO_3$ thin films, Applied Physics Letters 96 (2010) 131907–131909.

[45] S. Li, Y. Lin, B. Zhang, Y. Wang, C. Nan, Controlled fabrication of $BiFeO_3$ uniform microcrystals and their magnetic and photocatalytic behaviors, The Journal of Physical Chemistry C 114 (2010) 2903–2908.

[46] Z.S. Macedo, C.R. Ferrari, A.C. Hernandes, Impedance spectroscopy of $Bi_4Ti_3O_{12}$ ceramic produced by self-propagating high-temperature synthesis technique, Journal of The European Ceramic Society 24 (9) (2004) 2567–2574.

[47] J.-T. Han, Y.-H. Huang, X.-J. Wu, C.-L. Wu, W. Wei, B. Peng, W. Huang, J.B. Goodenough, Tunable synthesis of bismuth ferrites with various morphologies, Advanced Materials (Weinheim, Germany) 18 (2006) 2145–2148.

[48] A.Z. Simões, M.A. Ramírez, C.S. Riccardi, A.H.M. Gonzalez, E. Longo, J.A. Varela, Synthesis and electrical characterization of $CaBi_2Nb_2O_9$ thin films deposited on Pt/Ti/SiO_2/Si substrates by polymeric precursor method, Materials Chemistry and Physics 98 (2006) 203–206.